

# REPORT DOCUMENTATION PAGE

Form Approved  
OMB No. 0704-0188

Public reporting burden for this collection of information is estimated to average 1 hour per response, including the time for reviewing instructions, searching existing data sources, gathering and maintaining the data needed, and completing and reviewing the collection of information. Send comments regarding this burden estimate or any other aspect of this collection of information, including suggestions for reducing this burden, to Washington Headquarters Services, Directorate for Information Operations and Reports, 1215 Jefferson Davis Highway, Suite 1204, Arlington, VA 22202-4302, and to the Office of Management and Budget, Paperwork Reduction Project (0704-0188), Washington, DC 20503.

1. AGENCY USE ONLY (Leave blank)		2. REPORT DATE 28 Jul 1995	3. REPORT TYPE AND DATES COVERED Summary 01 Jun 1994 - 31 May 1995	
4. TITLE AND SUBTITLE Innovative Acoustic Techniques for Studying New Materials and New Developments in Solid State Physics (Includes ASSERT)			5. FUNDING NUMBERS PE 61153N G N00014-92-J-1186 G N00014-93-1-0779	
6. AUTHOR(S)  Julian D. Maynard				
7. PERFORMING ORGANIZATION NAME(S) AND ADDRESS(ES) The Pennsylvania State University Department of Physics 104 Davey Lab University Park, PA 16802			8. PERFORMING ORGANIZATION REPORT NUMBER	
9. SPONSORING/MONITORING AGENCY NAME(S) AND ADDRESS(ES) Office of Naval Research ONR 331 800 North Quincy Street Arlington, VA 22217-5660			10. SPONSORING/MONITORING AGENCY REPORT NUMBER	
11. SUPPLEMENTARY NOTES				
12a. DISTRIBUTION / AVAILABILITY STATEMENT  Approved for public release: Distribution unlimited			12b. DISTRIBUTION CODE	
13. ABSTRACT (Maximum 200 words)  The goals of this project involve the use of innovative acoustic techniques to study new materials and new developments in solid state physics. Major accomplishments include a) the submission of a Phys. Rev. Lett. paper on the use of resonant ultrasound spectroscopy (RUS) to determine the isotropy of a quasicrystal, b) the identification of a problem with the RUS analysis technique, c) the construction of a major facility for the study of fracture, and d) the preparation of a draft of a paper on a resonant photoacoustic technique.				
14. SUBJECT TERMS  Acoustics, Solid State Physics, Materials, Fracture			15. NUMBER OF PAGES 49	
			16. PRICE CODE	
17. SECURITY CLASSIFICATION OF REPORT UNCLASSIFIED	18. SECURITY CLASSIFICATION OF THIS PAGE UNCLASSIFIED	19. SECURITY CLASSIFICATION OF ABSTRACT UNCLASSIFIED	20. LIMITATION OF ABSTRACT	



19950814 004

JK

## **INNOVATIVE TECHNIQUES FOR STUDYING NEW MATERIALS AND NEW DEVELOPMENTS IN SOLID STATE PHYSICS**

This annual summary report presents the accomplishments for ONR grant N00014-92-J-1186, "Innovative Acoustic Techniques for Studying New Materials and New Developments in Solid State Physics". Progress was made in a) the use of resonant ultrasound spectroscopy (RUS) to study quasicrystals, b) the measurement of individual bond breaking events during the fracture of a brittle material, and c) the use of a resonant photoacoustic technique to measure infrared optical absorption in highly transparent materials.

### **Papers, Talks, etc.**

Progress with respect to papers, etc. includes the recent submission of a paper to Phys. Rev. Lett. (presented in Appendix A), the preparation of a draft of a paper for the J. Acoust. Soc. Am. (presented in Appendix B), and the preparation of drafts for several review papers, including an article for Physics Today and a tutorial on waves in disordered and quasiperiodic media. Four contributed papers were presented at meetings, and seven invited lectures were given. Animated images of the normal modes of elastically vibrating crystals were made available at a World Wide Web site (<http://www.phys.psu.edu/MAY-NARD/maynard.html>). In recognition of our research, the principal investigator was awarded the Silver Medal from the Acoustical Society of America.

During the past year the total research group has consisted of four graduate students (some with only partial ONR support) and two postdocs; a number of outstanding undergraduates have made significant contributions to our research. A list of the publications, personnel, etc. is presented in Appendix C.

In the sections which follow, a brief summary of the research accomplishments will be presented.

### **Measuring the Isotropy of a Quasicrystal with Resonant Ultrasound Spectroscopy**

One of the fascinating properties of quasicrystals is that, unlike conventional crystals, quasicrystals are elastically isotropic. For conventional crystals with high symmetries (e.g. cubic crystals), many physical properties are isotropic, but the property of linear elasticity is fundamentally anisotropic; that is, the velocity of sound may be different in different directions. Thus it is interesting that icosahedral quasicrystals, having long-range order like conventional crystals, must be isotropic in sound propagation. Quasicrystals are further interesting in that by attaining an appropriate amount of a unique strain (phason strain), they may be transformed into conventional crystals (referred to as "periodic approximants") and become anisotropic. Measuring these properties experimentally has been challenging, because while conventional crystals are fundamentally anisotropic, their elastic constants may be numerically very close to those of an isotropic material, so that it is difficult to distinguish between intrinsically isotropic and anisotropic behavior in a measurement. Indeed, nearly isotropic behavior might be expected in the periodic approx-

imants because they are structurally very similar to the isotropic quasicrystals. In our research we used resonant ultrasound spectroscopy to obtain high precision measurements of the elastic constants of both the quasicrystalline and periodic approximant phases of AlCuLi and found, with a significant level of confidence, that the quasicrystalline phase is isotropic (differing from the most nearly isotropic conventional crystal by ten standard deviations), while the periodic approximant is not. Details of this research are presented in Appendix A.

## Problems with Resonant Ultrasound Spectroscopy

Although the paper on the RUS study of quasicrystals was only recently submitted, the data were taken nearly a year ago. The reason for the delay was that a problem was discovered in the RUS analysis technique. In order to obtain more accurate results from the quasicrystal data, it was necessary to apply the RUS analysis not to a rectangular parallelepiped, as is usually done, but instead to a shape which deviated slightly, with faces departing from parallel and perpendicular by only tenths of a degree. It was found that the RUS analysis technique went unstable in this case, and considerable effort was required to determine the extent of the problem and its solution. Details of this study are presented below.

The effect of perturbations in boundary shape on the natural frequencies of vibrating systems is an important fundamental problem; Rayleigh[1] and Morse[2] both considered the problem of a membrane with a perturbed boundary, and Woodhouse[3] and others have considered the problem of a nearly spherical elastic solid, as this relates directly to the free vibrations of the spheroidal Earth. As mentioned above, the effects of shape perturbations are important to resonant ultrasound spectroscopy.

One challenging aspect of this problem has been that only certain geometries have analytic solutions, so that most shapes and boundary perturbations must be treated by approximate methods. The approximations may be non-trivial; Morse[2] has shown that inclining one side of a square membrane at a slight angle has a second-order effect on the frequencies, thus requiring second-order approximations. However, modern computing power makes it possible to use very accurate numerical methods based on variational principles, such as the Rayleigh-Ritz technique, to precisely calculate the natural frequencies of elastic solids in a wide variety of otherwise intractable geometries. The success of RUS is in part based on the use of Rayleigh-Ritz to calculate the frequencies of anisotropic cubes and rectangular parallelepipeds, the sample shapes which are the easiest to prepare. In 1991 Visscher[4] showed that Rayleigh-Ritz could also be used to compute the frequencies of elastic solids whose boundaries were not level surfaces of a separable coordinate system. This suggested that Rayleigh-Ritz could be used to systematically evaluate the effects of slightly nonparallel or nonperpendicular faces on the frequencies of the nearly parallelepiped samples used in RUS, by direct calculation. We undertook such an investigation, in particular to determine the importance of shape deviations on the very sensitive anisotropy measurement for a quasicrystal (see Appendix A).

<input checked="" type="checkbox"/>	
<input type="checkbox"/>	
<input type="checkbox"/>	
11/20/2007/ JF?	
Availability Codes	
Serial no./cp	
Dist	Specs
A-1	

The details of applying the Rayleigh-Ritz technique to RUS are available in the literature[4]. The relevant result is that the problem reduces to solving a matrix eigenvalue problem.

$$\Gamma a = \omega^2 E a \quad (1)$$

where  $\Gamma$  is a symmetric matrix,  $E$  is a positive definite symmetric matrix,  $\omega^2$  is the eigenvalue, and  $a$  is an eigenvector. The size and form of the matrices depend on the number and type of basis functions used in the Rayleigh-Ritz approximation. With a large enough basis set, very accurate values of  $\omega$  can be obtained, at the cost of diagonalizing very large matrices. In the past, computational efficiency was emphasized in applying this method to RUS, so basis sets were carefully chosen to exploit symmetries in sample shapes and crystal lattices, in order to block-diagonalize the matrix problem. Visscher's insight was that if a very simple set of basis functions (powers of cartesian coordinates) is used, the matrix element integrals can still be done analytically for a wide variety of shapes (often at the cost of solving a larger matrix), and therefore many boundary value problems previously thought intractable are readily solved with Rayleigh-Ritz. The basic formulation of Rayleigh-Ritz does not contain any apparent restrictions on boundary shape, crystal symmetry, or even sample homogeneity, and indeed Visscher[4] obtained numerical eigenvalue solutions for vibrating cones, cylinders, triangular prisms, anisotropic ellipsoids, sandwiches of differing materials, and other seemingly pathological cases.

It seemed simple enough, then, to apply this technique to a perturbed parallelepiped, and we set about calculating the natural frequencies of a nearly rectangular parallelepiped, with sides flaring out slightly so that it formed a "rhombic prism". The evaluation of the matrix elements was straightforward, but to our surprise the solution exhibited very anomalous and singular behavior.

Our first difficulty came when a commercial eigenvalue routine (DSYGV in the ESSL library for IBM mainframes) rejected the matrix  $E$  from Eq. 1 as "not positive definite"; theory says it must be (and an independent numerical check confirmed that it was). Concerned that the matrix  $E$  was ill-conditioned, we set about reformulating Eq. 1 using singular value decomposition (SVD), to diagnose the extent of the conditioning problem. We first use SVD to take the "square root" of the matrix  $E$ , noting that the singular values of a positive definite symmetric matrix must be positive:

$$E_{ij} = \sum_k F_{ik} s_k F_{jk} = \sum_k G_{ik} G_{jk} \quad (2)$$

where  $G_{ij} = \sqrt{s_i} F_{ji}$ . We define  $\bar{G}_{ij} = (1/\sqrt{s_i}) F_{ji}$ , and note that  $\bar{G}G^T$  and  $\bar{G}^T G$  yield the identity matrix. The ratio of the smallest to the largest singular value  $s$  will provide a measure of the conditioning of the matrix  $E$ . Eqn. 1 can be transformed to

$$\Gamma' b = \omega^2 b \quad (3)$$

where  $\Gamma' = \bar{G}\Gamma\bar{G}^T$  is a symmetric matrix and the vector  $b = Ga$ . Since  $\Gamma'$  is symmetric, we can perform SVD on it and the singular values will be the eigenvalues. Furthermore, the ratio of the smallest to the largest singular value will provide a measure of the conditioning of this part of the matrix problem.

With proper normalization of the basis functions, the problem appeared to be sufficiently well-conditioned for a solution using double precision. However, even when the sides were given a very modest tilt,  $\theta = 0.02^\circ$ , spurious extra mode frequencies would appear. The eigenvectors for these spurious modes were used to produce computer animations of the modes themselves, and these animations confirmed that the modes were highly unphysical (some of our animations may be obtained from the WWW site mentioned earlier) Fig. 1 shows a graph of a few eigenfrequencies versus tilt angle; clearly the solution is unstable.

We decided to confine our attention to small tilt angles and only calculate the matrix elements to first order in  $\theta$ . Fig. 2 shows that this solution is much more stable. Concurrently we made another interesting discovery: if the coordinates used in evaluating the matrix elements are rotated so that the trapezoid appears as four adjacent triangular prisms, the solution is completely stable (unfortunately, this only works for a shape which is nominally square to begin with). Fig. 3 shows the first order solution compared to the "prism" solution, which are in excellent agreement for small angles.

Having obtained an apparently stable solution for small angles, we commenced an investigation on the effects of shape perturbation on the elastic constant determination in RUS. In the RUS analysis, computed and observed frequencies are compared iteratively while the elastic constants are adjusted, until the differences between the computed and observed frequencies are minimized. We used frequencies for a perturbed shape as the "observed" frequencies, but assumed a perfect rectangular parallelepiped shape (with the same volume) in the RUS analysis. To our surprise, even though there were no large anomalies in the frequencies, there were sharp anomalies in the elastic constant determination. This is particularly evident in the anisotropy parameter, a ratio of elastic constants that expresses the anisotropy of a cubic substance. Fig. 4 shows the apparent elastic anisotropy versus tilt angle, for a particular fictitious specimen (which was elastically isotropic). The singular artifact is evident around  $0.6^\circ$ .

Our immediate goal in this investigation was to determine the effect of shape perturbation on the measurement of quasicrystal anisotropy, so at this point we carefully measured the relative angles between all the sides of our quasicrystal sample, to see whether they were sufficiently small to expect a stable solution. The angles turned out to be all less than  $0.3^\circ$ , but the sample had tilts in more than one dimension, which meant we were unable to directly calculate the normal modes for its shape. However, we did find a working solution for this particular sample. Morse[2] argues that a tilted boundary produces a second-order perturbation in the eigenvalues; this was confirmed in our case by applying a first-order

theory similar to that of Woodhouse[3], and obtaining zero shifts in the frequencies. We therefore assumed that for small angles, we could sum the independent contributions of the tilts in each dimension, by calculating the second-order coefficients for each frequency, for each separate tilt, i.e.,

$$f_j \rightarrow f_j + \sum_i \alpha_{ij} \theta_i^2 \quad (4)$$

where the  $\alpha_{ij}$  are determined from calculations using small angles, and the  $\theta_i$  are the angles between the sample sides. The success of this approach is evident in our paper in Appendix A.

### Acoustic Studies of Brittle Foam Fracture as a Model for Current Theories in Statistical Physics

While studies of fracture have been undertaken for many years, most of the research has involved taking data and developing models for the purpose of predicting a critical size crack which would grow catastrophically under a design load for a given structure. Recently, theorists from condensed matter physics have recognized an analogy between fracture and contemporary physics problems in directed polymer growth in a random medium, viscous fingering, diffusion limited aggregation, self-organized criticality, and other problems in pattern formation. The theory for the analogies involves the statistical physics of random systems. The brittle material is modeled as a network of bonds which are distributed randomly in the network with some probability distribution. Fracture is simulated by applying a stress or strain at the boundaries of the bond network; at some value of the boundary load, one of the internal bonds will break, increasing the load on the remaining bonds, and the process continues until the sample breaks in two. The physical properties which are calculated with such models include the distribution of the stress just prior to breaking, the critical acceleration of the crack at the beginning of fracture, and the scaling of such quantities with the cross sectional area of the system.

In order to provide a test of the theories, it is necessary to have a measurement which can detect individual bonds breaking during the catastrophic fracture. For the usual materials used in the study of fracture (glasses and resins), it would be impossible to detect individual atomic bonds breaking. However, it would be possible in a macroscopic model of a brittle solid. For this purpose we have been studying an open cell carbon foam material having struts with lengths on the order of 1-2 mm. The struts play the role of the random bonds in the statistical physics models. When this material is placed in water, the water completely permeates the sample, and sound from a breaking interior strut easily propagates through the water in the open sample to a transducer outside the sample. With this system, we are able to measure, as a function of time and applied stress, precursors and their distributions in amplitude and time, the statistics of the individual bond breaking events during the cascade at the catastrophic fracture, the fractal nature of the fracture surface, etc.

A major accomplishment has been the construction of a facility for performing the fracture

measurements. As illustrated in Fig. 5, this is a versatile large scale apparatus, able to produce and sustain up to 2 tons of uniform tensile force for samples ranging from a few centimeters to 25 cm in diameter. The sample to be fractured is centered in a 1 m<sup>3</sup> tank of water, and a strain gauge on one of the supporting cables monitors the sample stress. Using several small 20 MHz transducers, detailed signals from the entire fracture process may be recorded. The complete fracture process consists of a train of intermittent precursor bursts, each consisting of one or several individual bond breaking events, followed by the final catastrophe which ruptures the sample into two pieces. The acoustic signals from such a fracture process have been captured with the use of two high frequency digital oscilloscopes which can collect a large number of time series in sequence and/or parallel. A typical record, showing precursors as well as the final catastrophe, is shown in Fig. 6. The fracturing statistics are being analyzed to look for dynamical effects, such as paired bond breaking events occurring on the same time scale as the internal reflection of stress waves. The complete set of statistics is being related to the applied tensile force, which is recorded for the entire fracture process.

In addition to the statistics of the precursors, etc., the fractal dimension of the rupture surface is being measured, using a "slit island" technique. A white plaster cast of the fracture surface is made, painted black, and then partially sanded on a flat surface. The remaining painted region shows the contour at that level. The remaining painted regions at a sequence of levels are imaged with a CCD camera, converted to computer bitmaps, and the perimeter and area of the contours are determined. A log-log plot of area versus perimeter for all of the levels yields the fractal dimension of the fracture surface.

To exploit the adaptability of the fracture facility, different materials have been studied. The tearing and separation of velcro has been found to be an example of "soft" elastic fracture with an acoustic emission pattern distinct from that of brittle carbon. Velcro could be an ideal material from which to construct detailed earthquake models, which also involve the fracturing of elastic media. Current earthquake models are usually computer simulations which suffer from the artifacts of finite element calculations, or lack detailed structure and hence cannot generate earthquake statistics comparable to those generated by actual earthquakes. Complex earthquake models could be easily studied with the fracture facility.

All of the results will provide well characterized data for theories of self-organized criticality.

### **Accomplishments in the Infrared Resonant Photoacoustics Project**

As discussed in previous progress reports, we have used both piezoelectric film (PVDF) and conventional LiNb transducers in a resonant photoacoustics apparatus, and have obtained the lowest optical absorption ever measured in a solid. An important aspect of the technique was that piezoelectric samples, such as quartz, produced large, easily detected signals in the transducers, as a consequence of the electric fields produced by the sample itself. For non-piezoelectric and highly transparent samples, such as calcium fluoride, the photoacoustic signal, even with a high Q resonance, is very weak. We have finally obtained

satisfactory results, and have prepared a draft of a paper for submission to the J. Acoust. Soc. Am., which is included in Appendix B. The graduate student, Wei-li Lin, presented an invited talk on these results at the May 1995 meeting of the Acoustical Society.

### Current and Other Funding

Other research grants include:

1. NSF Division of Materials Research, Condensed Matter Physics Program, DMR 93-06791, which includes 1 man-month of the principal investigators time.
2. ONR, Physics Division, September 15, 1993 to September 14, 1996, 180,000/3 yr, "Anisotropic heat exchanger/stack configurations for thermoacoustic heat engines"; includes 1 man-month of time for the principle investigator, distributed over 12 months.

### References

- [1] J. W. S. Rayleigh, *Theory of Sound* (Dover, New York, 1945) p. 209.
- [2] P. M. Morse and H. Feshbach, *Methods of Theoretical Physics* (McGraw- Hill, New York, 1953) p. 1062.
- [3] J. H. Woodhouse and F. A. Dahlen, *Geophys. J. R. Astr. Soc.* **53** , 335 (1978).
- [4] W. M. Visscher, A. Migliori, T. M. Bell, and R. A. Reinert, *J. Acoust. Soc. Am.* **90**, 2154 (1991).

### Figure Captions

Fig. 1. Some of the lower normal mode frequencies of a "trapezoidal prism", calculated using full polynomial expansion for the elements of the matrices in the Rayleigh-Ritz eigenvalue problem.

Fig. 2. Same as Fig. 1., except that the matrix elements are only calculated to first order in  $\theta$ .

Fig. 3. A comparison of two different solutions of the same eigenmode, one the first-order solution of Fig. 2., the other a solution obtained by creating the same sample from four adjacent triangular prisms.

Fig. 4. Apparent elastic anisotropy in RUS analysis caused by trapezoidal tilt in one dimension of an isotropic sample, versus tilt angle.

Fig. 5. The fracture facility, including: a large water tank, for the undisturbed propagation and detection of acoustic signals; hydraulic jacks, for lifting the cross beam and delivering up to 2 tons of tensile force to the sample held in the center of the tub; and a strain gage,

attached to a suspending element, which measures the force applied at the moment of each acoustic signal.

Fig. 6. Sequence mode collection of acoustic signals generated from the fracture of a 7 cm diameter carbon foam sample. The separate sequences are collected intermittently but displayed periodically.

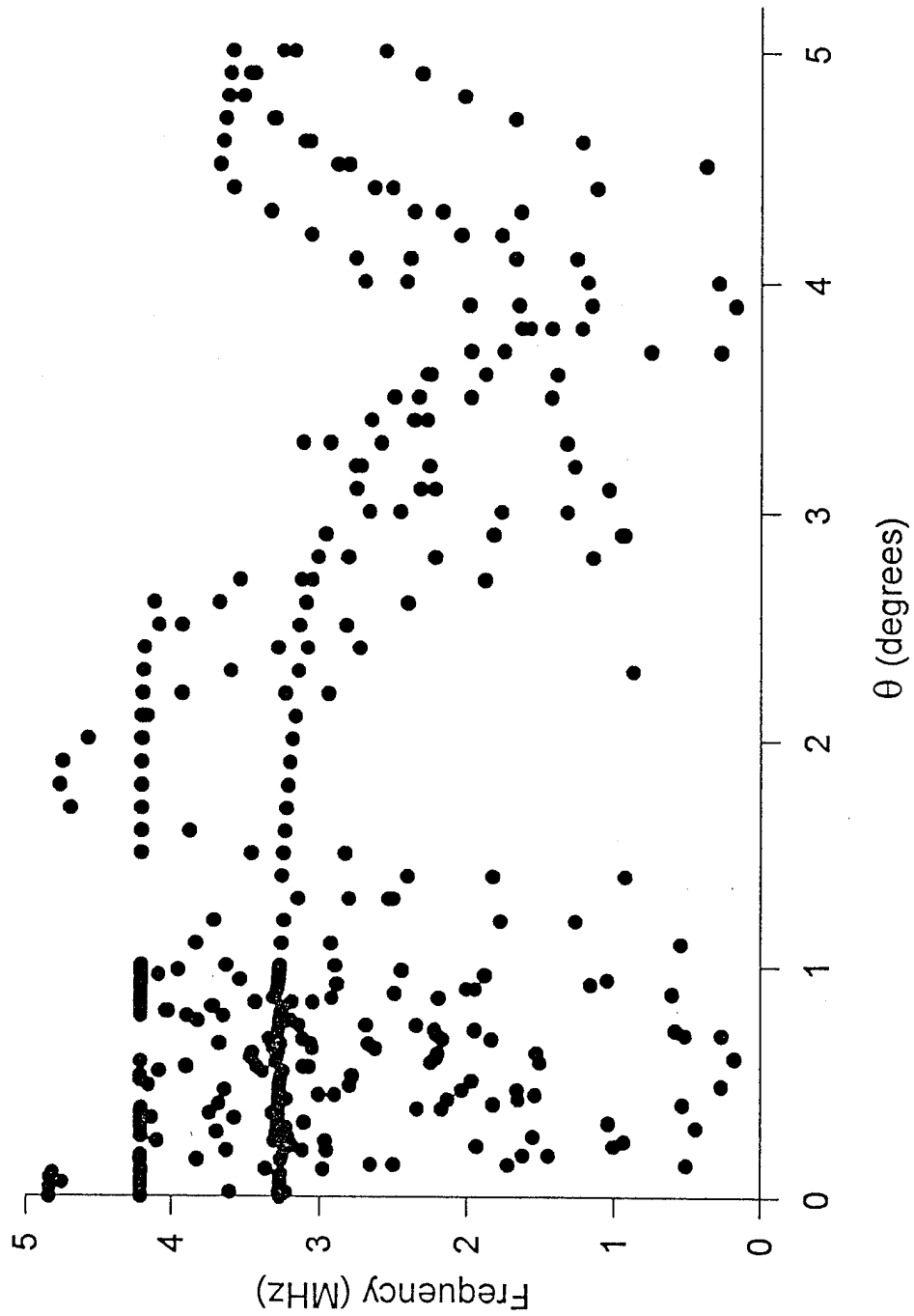
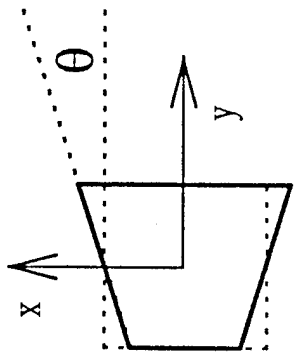


Fig. 1

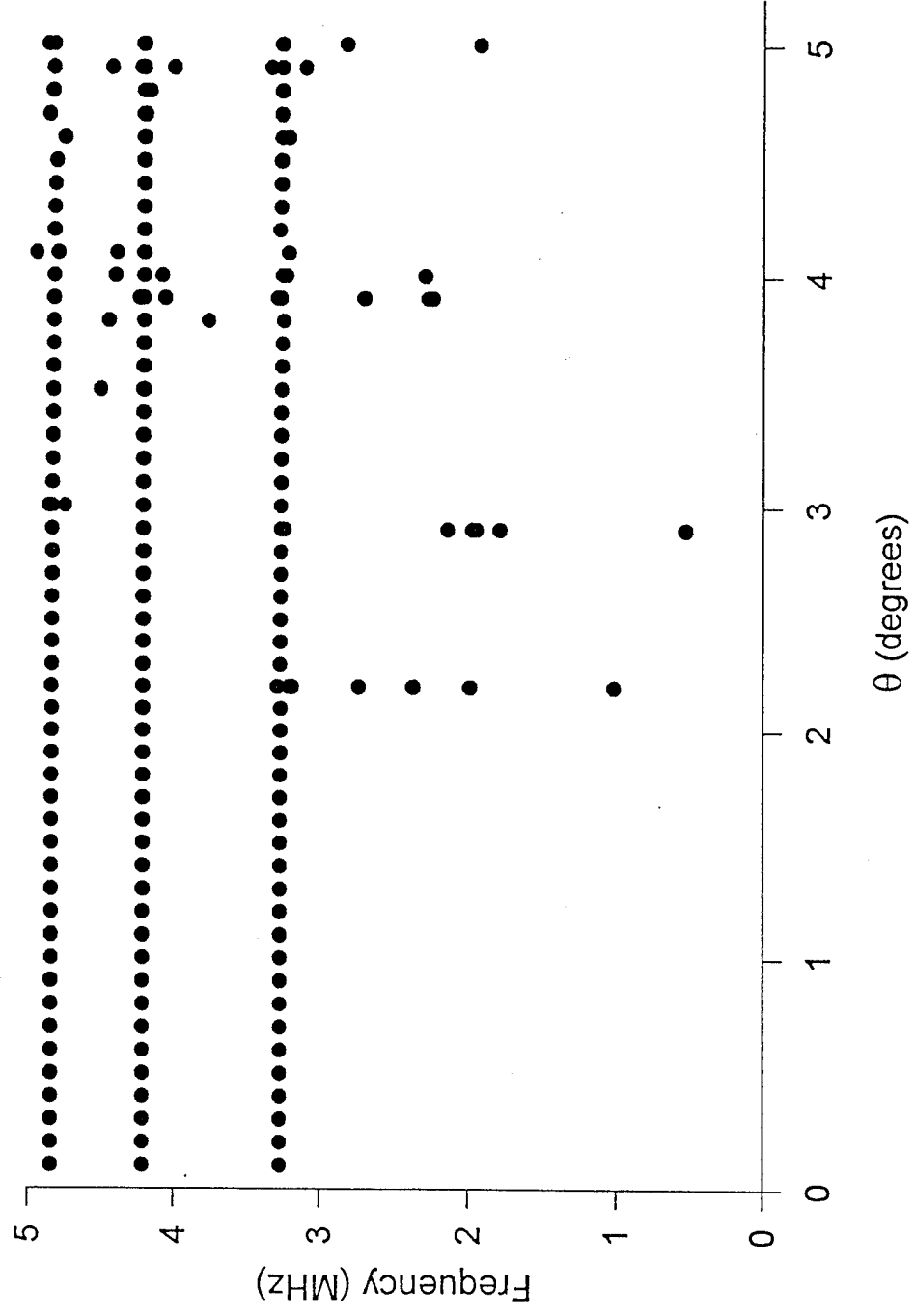
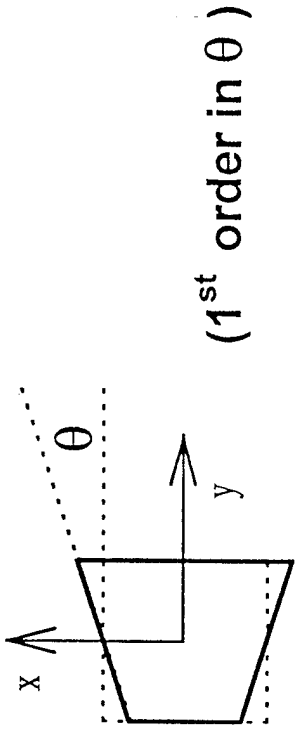
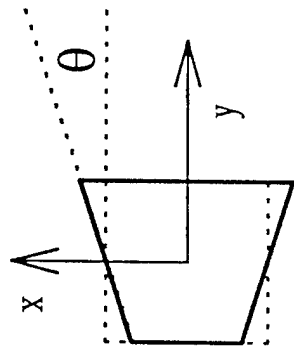


Fig. 2





( First order in  $\theta$  )

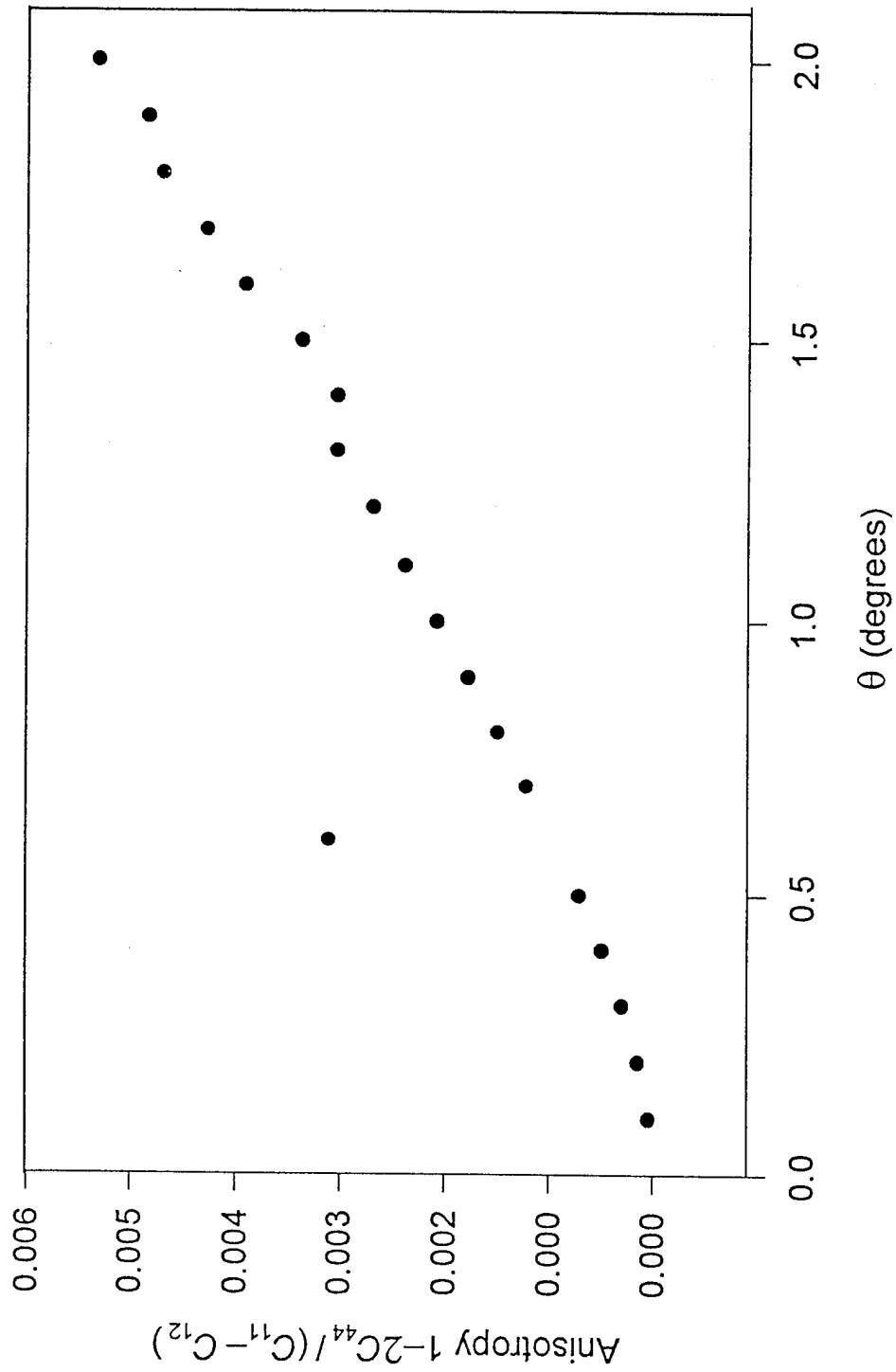


Fig. 4

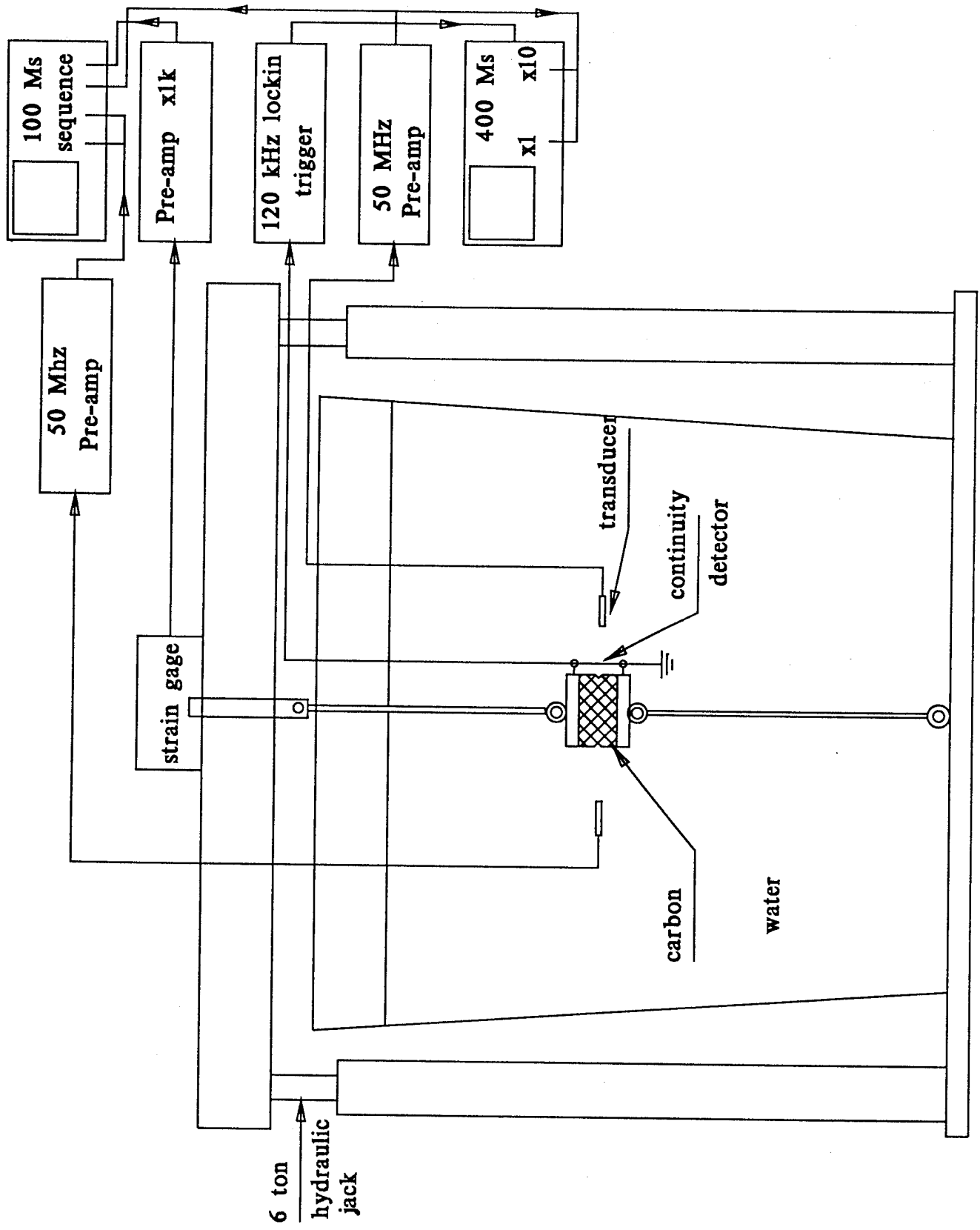
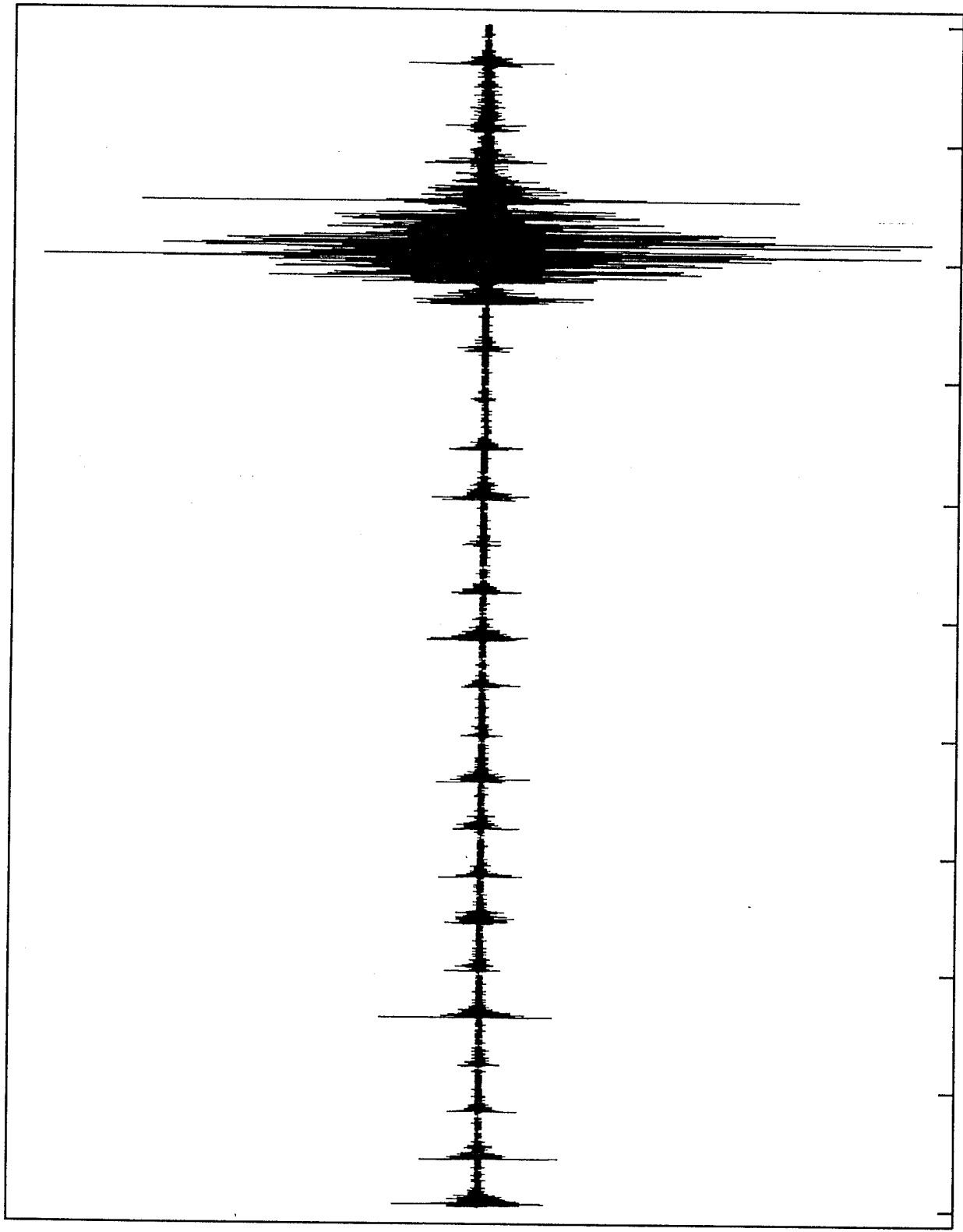


Fig. 5



received signal (arb. units)

time (0.5 ms/div)

Fig. 6

# Appendix A.

## Elastic Isotropy and Anisotropy in Quasicrystalline and Cubic AlCuLi

P. S. Spoor and J. D. Maynard

*Department of Physics, the Pennsylvania State University, University Park, Pennsylvania 16802*

A. R. Kortan

*AT&T Bell Laboratories, Murray Hill, New Jersey, 07974*

(June 22, 1995)

### Abstract

Unlike conventional crystals, quasicrystals are predicted to be elastically isotropic. To confirm this prediction experimentally, one must distinguish the quasicrystal from nearly isotropic crystals, which requires a high degree of precision. In this Letter, we report the use of resonant ultrasound spectroscopy to determine that the AlCuLi quasicrystal is isotropic within 0.07%, significantly more isotropic than any conventional crystal (by 10 standard deviations). By contrast, we find that a closely related cubic phase of AlCuLi is slightly, but measurably, anisotropic.

61.44,62.20

Typeset using REVTeX

One of the fascinating properties of quasicrystals [1] is that, unlike conventional crystals, quasicrystals are elastically isotropic [2]. For conventional crystals with high symmetries (e.g. cubic crystals), many physical properties are isotropic, but the property of linear elasticity is fundamentally anisotropic [3]; that is, the velocity of sound may be different in different directions. Thus it is interesting that icosahedral quasicrystals, having long-range order like conventional crystals, must be isotropic in sound propagation. Quasicrystals are further interesting in that by attaining an appropriate amount of a unique strain (phason strain) [2], they may be transformed into conventional crystals (referred to as “periodic approximants”) [4], thereby becoming elastically anisotropic. Measuring these properties experimentally has been challenging [5–7], because while conventional crystals are fundamentally anisotropic, their elastic constants may be numerically very close to those of an isotropic material, so that it is difficult to distinguish between intrinsically isotropic and anisotropic behavior in a measurement. Indeed, nearly isotropic behavior might be expected in the periodic approximants, because they are structurally very similar to the isotropic quasicrystals [8]. In this Letter we report the use of resonant ultrasound spectroscopy [9,10] to obtain high precision measurements of the elastic constants of both the quasicrystalline and a periodic approximant phase of AlCuLi and find, with a significant level of confidence, that the quasicrystalline phase is isotropic (differing from the most nearly isotropic conventional crystal by ten standard deviations), while the periodic approximant is not.

Before presenting the details of our measurement, it is worthwhile to quantify the difficulty of determining whether or not a material is elastically isotropic. For this purpose, we consider cubic tungsten, which has the smallest anisotropy for a conventional crystal to be found in the literature [11,12]. The sound velocity in tungsten varies with direction by less than 0.5%; depending on the orientations used in a particular experiment, the observable variation could be significantly smaller. To show that a quasicrystal is more isotropic than ordinary crystals, a sound velocity measurement would have to probe all principal directions (which might require remounting transducers, possibly resulting in a loss of precision) with an overall resolution better than 0.5%. This is especially challenging considering the small

size of most high-quality samples. Previous studies of quasicrystals [5-7] have found isotropy in sound propagation but only at the 1% level; considering the properties of tungsten and the possibilities for periodic approximants, it is apparent that more precise measurements are necessary. As will be discussed below, resonant ultrasound spectroscopy probes all principal directions in one measurement, while achieving precision sufficient both to show that the AlCuLi quasicrystal is at least an order of magnitude more isotropic than tungsten, and to quantify the anisotropy of a periodic approximant. First we shall discuss the notion of elastic anisotropy in terms of the elements of the elastic tensor.

The elastic tensor  $c_{ij}$  for an isotropic solid has only two independent elements, related to a shear and a bulk modulus. By contrast, the most symmetric elastic tensor for a conventional crystal (cubic) has three independent constants,  $c_{11}$ ,  $c_{12}$  and  $c_{44}$ , using conventional notation [3]. However, the form for the isotropic and cubic tensors are identical, except that for an isotropic solid,  $c_{12} = c_{11} + 2c_{44}$  [3]. It is therefore convenient to define an anisotropy parameter  $\epsilon$  as

$$\epsilon = 1 - \frac{2c_{44}}{c_{11} - c_{12}}, \quad (1)$$

so that  $\epsilon$  is zero for an isotropic solid. For tungsten,  $\epsilon$  is only  $0.007 \pm 0.002$  [11,12].

Verifying small values of  $\epsilon$  not only requires a precise measurement of the elastic constants, but also requires single crystal (or quasicrystal) samples of very high quality, since defects or grain boundaries could give rise to systematic errors, resulting in a spurious anisotropy result. For our measurement we used the AlCuLi system, because high-quality single crystals of both the quasicrystal and a periodic (cubic) approximant can be grown to millimeter size [13]. The cubic approximant, referred to as R-phase, is a bcc lattice of essentially icosahedral units, and is similar in structure, composition, and density to the quasicrystalline phase [8,14]. A 1 mm-thick disk of AlCuLi cut from an ingot of approximately 1 cm diameter, containing R-phase and quasicrystalline phase, was prepared at AT&T Bell Laboratories. Two specimens, one of each phase, were cut from this disk with a diamond wire saw, and polished into rectangular parallelepipeds. At first, a few features (possibly

fissures or grain boundaries) were observed on the sample surfaces. As a consequence, the specimens were painstakingly polished, examined, and repolished until no surface features were visible. Care was taken to insure that the sample faces were flat, smooth, and perpendicular to within  $0.5^\circ$ . The finished parallelepipeds of cubic and quasicrystalline AlCuLi were approximately  $1.0 \times 0.7 \times 0.4$  mm and  $0.6 \times 0.4 \times 0.4$  mm, respectively. The finished samples were each small enough to be placed entirely within a  $1 \text{ mm}^2$  X-ray beam, and transmission Laue diffraction revealed that they were both single crystals of excellent quality. A third parallelepiped,  $0.4 \times 0.2 \times 0.3$  mm, with a mass of only  $\sim 70 \mu\text{g}$ , was prepared from a separate sample of quasicrystalline AlCuLi for comparison. Laue photographs of this third specimen, however, showed that more than one grain may have been present. Henceforth these samples shall be referred to as R (R-phase cubic approximant), QX1 (high quality quasicrystal), and QX2 (lesser quality quasicrystal). The anisotropies of all three samples were determined using resonant ultrasound spectroscopy.

In resonant ultrasound spectroscopy [9,10], a specimen's normal mode frequencies of free vibration are used along with its shape and mass to determine its elastic properties. In the present measurement, a rectangular parallelepiped sample is held lightly at opposing corners between two broadband transducers, one a driver and the other a receiver, as shown in Fig. 1. Since the quasicrystal samples are brittle and may have a mass as small as  $70 \mu\text{g}$ , we employ a polyvinylidene flouride (PVDF) piezoelectric film transducer [9], with a thickness of only  $9 \mu\text{m}$ , which minimizes contact force and damage to fragile sample corners. The driver frequency is swept and the response at the receiver is monitored with a phase-sensitive detector and digitized. The quality factors of the sample resonances are relatively high, between  $10^3$  and  $10^5$ . An initial scan to locate the peaks is followed by a finer scan of each peak; each peak is then fit with a Lorezian, allowing  $10^{-4}$  or better precision in frequency determination, even for weak signals. The lowest 31 resonances of QX1 were recorded, with somewhat fewer recorded for QX2 and R. Since individual normal modes may involve torsion, shear, dilatation, or a combination, along any axis, all principal directions are investigated in several ways with a single spectrum, if enough modes are used.

Once a spectrum of  $N$  observed resonance frequencies  $f_i^o$  ( $i = 1, N$ ) has been obtained, a Levenberg-Marquart algorithm is used to fit the data by varying the free parameters, such as elastic constants, until a figure-of-merit  $F$  is minimized. Following Ref. [10], we minimize

$$F = \sum_{i=1}^N \left( \frac{f_i^o - f_i^t}{f_i^o} \right)^2, \quad (2)$$

where the  $f_i^t$  are theoretical frequencies calculated according to the variational method used by Demarest [15] and improved by Ohno [16] and Visscher [17]. Once  $F$  has been minimized, the goodness of the fit can be specified by the rms error  $(F/N)^{1/2}$ , which is approximately equal to the average error in fitting each frequency.

We assume in our fitting procedure that all of our samples have at least cubic symmetry, so that there are at most three independent elastic constants. If the quasicrystal is isotropic and has only two independent constants, the value of  $\epsilon$  from Eq. (1) will be correspondingly small. The frequencies in the measurement are determined with good precision and accuracy, so that the accuracy of the calculated elastic constants is limited by the accuracy with which the geometry of the sample is determined. The size of the sample may be taken as one physical dimension and two aspect ratios. Since we measure many more frequencies than elastic constants, the problem is overdetermined and the aspect ratios can be included as free parameters in the fit. Only a single dimension is required to determine the elastic constants, but in calculating the anisotropy parameter with a ratio of elastic constants, the dimension, as well as the mass of the sample, cancels out. Error can occur if the actual shape of the sample differs in a systematic way from that assumed in the fitting program, nominally a rectangular parallelepiped. An inexact shape may result from the limits of our polishing technique and the small size of the samples, and shape anisotropy may appear as elastic anisotropy in the results of a fitting procedure that assumes an ideal shape. For a carefully shaped sample, the sides may differ from being mutually perpendicular by a few tenths of a degree, and the errors in  $c_{ij}$  may be a few tenths of a percent [10], sufficiently small for most purposes. However, the present measurement requires as little systematic error as possible, so we measured the actual shape of QX1 by first mounting the sample on a goniometer, and

used a laser beam reflecting from the polished sample faces to determine the angles between each side. A second-order frequency perturbation calculation using this more accurate shape is included when fitting the data from QX1. For the R sample, the shape was sufficiently rectangular and the anisotropy was sufficiently large that such fine-tuning was unnecessary.

The resulting elastic constants  $c_{11}$ ,  $c_{12}$ ,  $c_{44}$ , anisotropy  $\epsilon$ , and rms error for all three samples are given in Table I, and the anisotropy results are further summarized in Fig. 2, which shows the rms error and the anisotropy, with the standard deviations indicated with error bars. The rms errors for all three data sets are  $\leq 0.1\%$ , indicating an excellent agreement between observed and predicted resonance frequencies, and a high degree of confidence in the overall fits. The standard deviations for  $\epsilon$  were obtained by a Monte Carlo method, with the width of the scatter in the synthetic data sets based on the residuals  $|f_i^o - f_i^t|$  in the fit to the actual data. The standard deviations (and the error bars in Fig. 2) reflect to some degree the sample quality and the number of data points; the error for the high quality quasicrystal (QX1) is concomitantly the smallest of the three, while the error for QX2 (suspected to be more than one grain) is the greatest. It is apparent that the R-phase is measurably anisotropic, while the quasicrystal samples are not. The anisotropy of the R-phase is seen to be comparable to that of tungsten, and differs from zero by seven standard deviations. The anisotropy of the high quality quasicrystal, with  $\epsilon = 0.0002 \pm 0.0007$ , is 10 standard deviations, or about a factor of 10, smaller than the anisotropy of tungsten. Hence the quasicrystal is significantly more isotropic than the most isotropic conventional crystal to be found in the literature.

An additional test for isotropy can be performed by presuming various crystal orientations, other than the one initially assumed, in the theoretical frequency calculations [10]; i.e. one uses an elastic tensor that has been rotated relative to the axes of the crystal lattice. In this way, one can test whether crystal misorientation affects how well the data are fit by the model. If a crystal is high quality and anisotropic, one should notice a minimum in the fit error when the elastic tensor is correctly aligned with the the lattice. Plots of the figure-of-merit  $F$  versus rotation of the elastic tensor in two of the three Euler angles show that the

cubic phase has a clear dependence on orientation, while the quasicrystal shows none. The minimum in  $F$  for the cubic phase is along a principal direction, important evidence that its anisotropy is due to its crystal structure and is not an artifact of sample quality.

It is of interest to calculate the maximum variation in sound velocity one could expect to observe in the cubic R-phase of AlCuLi, due to its small, but finite, anisotropy. We find that the cubic phase has a maximum sound velocity variation of 0.6%, which could not be detected by a measurement with a resolution of 1%.

In conclusion, we have shown the AlCuLi quasicrystal to be isotropic with  $\epsilon = 0.0002 \pm 0.0007$ , significantly more isotropic than conventional crystals, in accordance with theoretical predictions. The R-phase periodic approximant has been shown to possess an anisotropy which is very small, but readily measured with resonant ultrasound spectroscopy. In future research other quasicrystal alloys and their periodic approximants could be investigated, including studies of the temperature and pressure dependence of their elastic constants. The latter measurement might provide evidence of anisotropy in the higher-order elastic constants for the quasicrystal, as predicted by theory [18], and would provide additional evidence for intrinsic isotropy in the linear elastic constants. That is, while conventional crystals may be made isotropic under the right conditions of pressure and temperature [11], the quasicrystal should remain isotropic at all conditions for which it is stable.

The authors would like to thank Earl Ryba and Bob Greene for helpful discussions and assistance with sample characterizations. We also thank Bill Visscher for his advice regarding the numerical computations. This work was supported in part by NSF grants DMR-9000549, DMR-9306791, and the Office of Naval Research.

## REFERENCES

- [1] D. Shechtman, I. Blech, D. Gratias, and J. W. Cahn, *Phys. Rev. Lett.* **53**, 1951 (1984);  
D. Levine and P. J. Steinhardt, *Phys. Rev. Lett.* **53**, 2477 (1984).
- [2] Per Bak, *Phys. Rev. B* **32**, 5764 (1985).
- [3] For a general reference, see R. Truell, C. Elbaum, and B. Chick, *Ultrasonic Methods in Solid State Physics* (Academic Press, New York, 1969).
- [4] A. Yamamoto, *Phys. Rev. B* **45**, 5217 (1992).
- [5] G. A. M. Reynolds, B. Golding, A. R. Kortan, and J. M. Parsey, Jr., *Phys. Rev. B* **41**, 1194 (1990).
- [6] S. Satish, A. Kulik, and G. Gremaud, *Sol. St. Comm.* **77**, 403 (1991).
- [7] A. I. Goldman, C. Stassis, M. de Boissieu, R. Currat, C. Janot, R. Bellissent, H. Moud-  
den, and F. W. Gayle, *Phys. Rev. B* **45**, 10280 (1992).
- [8] C. L. Henley, *Phys. Rev. B* **43**, 993 (1991).
- [9] J. D. Maynard, *J. Acoust. Soc. Am.* **92**, 1754 (1992).
- [10] A. Migliori, J. L. Sarrao, W. M. Visscher, T. M. Bell, Ming Lei, Z. Fisk, and R. G.  
Leisure, *Physica B* **183**, 1 (1993).
- [11] F. H. Featherston and J. R. Neighbors, *Phys. Rev.* **130**, 1324 (1963).
- [12] See D. H. Chung and W. R. Buessem, in *Anisotropy of Single-Crystal Refractory Com-  
pounds*, edited by F.W. Vahliek and S. A. Mersol (Plenum Press, New York, 1968) p.  
217, and A. G. Every and A. K. McCurdy, in *Landolt-Börnstein Tables, New Series,  
Group III (Crystal and Solid State Physics)* volume **29a**, edited by O. Madelung and  
D. F. Nelson (Springer-Verlag, Berlin, 1992) p. 11. For the anisotropy of tungsten and  
its standard deviation, we use the average of the values in the literature. Published  
anisotropies for some crystals are smaller than that of tungsten, but the uncertainties

in the elastic constants are either too large or are not given. We consider only crystals at standard temperature and pressure; other conditions are discussed in the conclusions in the text.

- [13] A. R. Kortan, H. S. Chen, J. M. Parsey, and L. C. Kimerling, *J. Mat. Sci.* **24**, 1999 (1989).
- [14] C. Janot, *Quasicrystals: a Primer* (Oxford University Press, Oxford, 1992) p. 166.
- [15] H. H. Demarest, *J. Acoust. Soc. Am.* **49**, 768 (1971).
- [16] I. Ohno, *J. Phys. Earth* **24**, 355 (1976).
- [17] W. Visscher, A. Migliori, T. M. Bell, and R. A. Reinert, *J. Acoust. Soc. Am.* **90**, 2154 (1991).
- [18] L. C. Chen, S. Ebalard, L. M. Goldman, W. Ohashi, B. Park, and F. Spaepen, *J. Appl. Phys.* **60**, 2638 (1986).

## FIGURES

FIG. 1. A resonant ultrasound cell, showing a sample held at its corners between two thin piezoelectric film (PVDF) transducers. The strips are  $\sim 0.5$  mm wide, and aluminum evaporated on either side has a 0.5 mm overlap, creating a  $0.5 \text{ mm}^2$  active area (see Ref. [9]).

FIG. 2. The anisotropies of quasicrystalline and R-cubic AlCuLi. The vertical coordinate shows the rms error in fitting the frequency data for each sample. QX1 is a single quasicrystal; in QX2 more than one grain may be present.

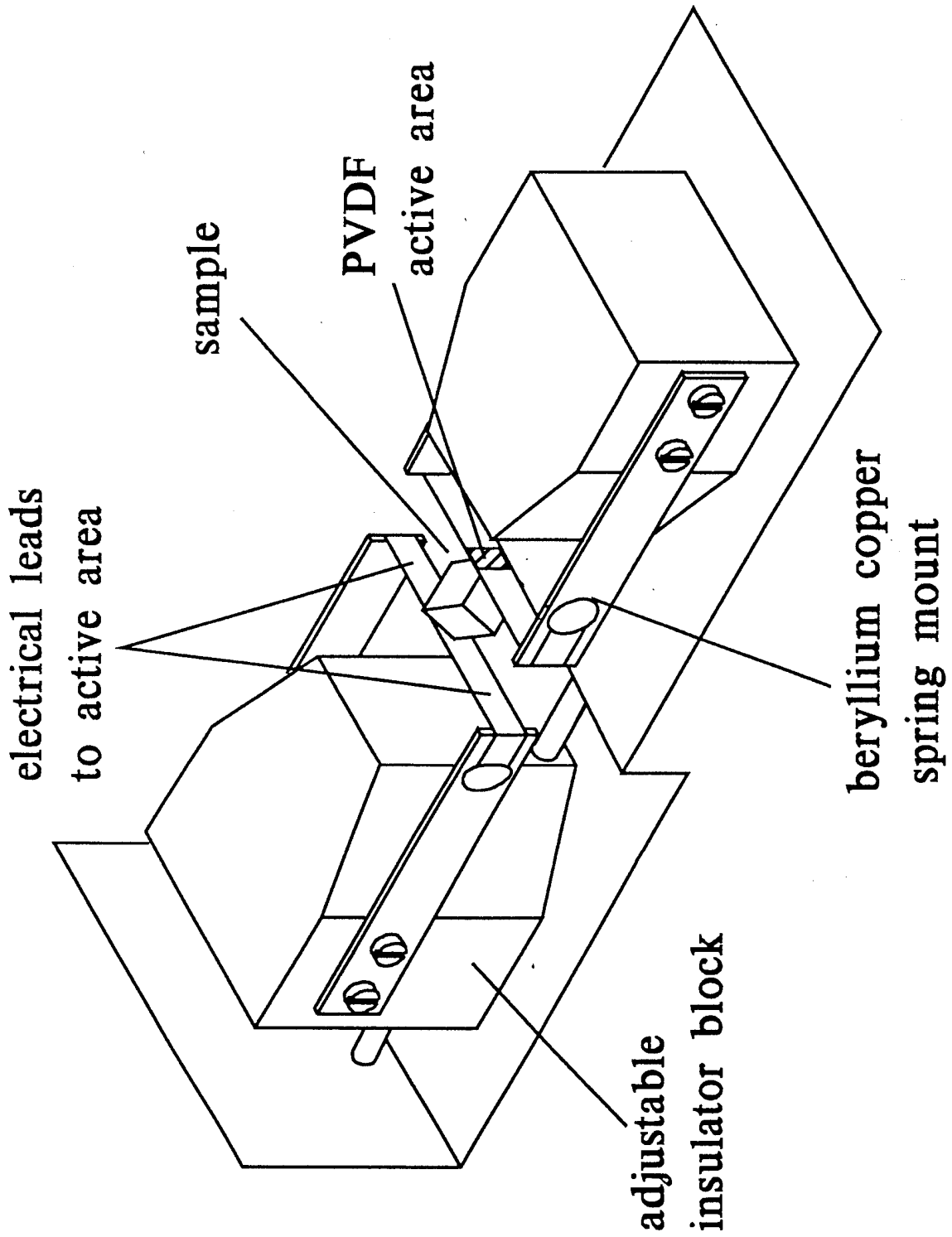
## TABLES

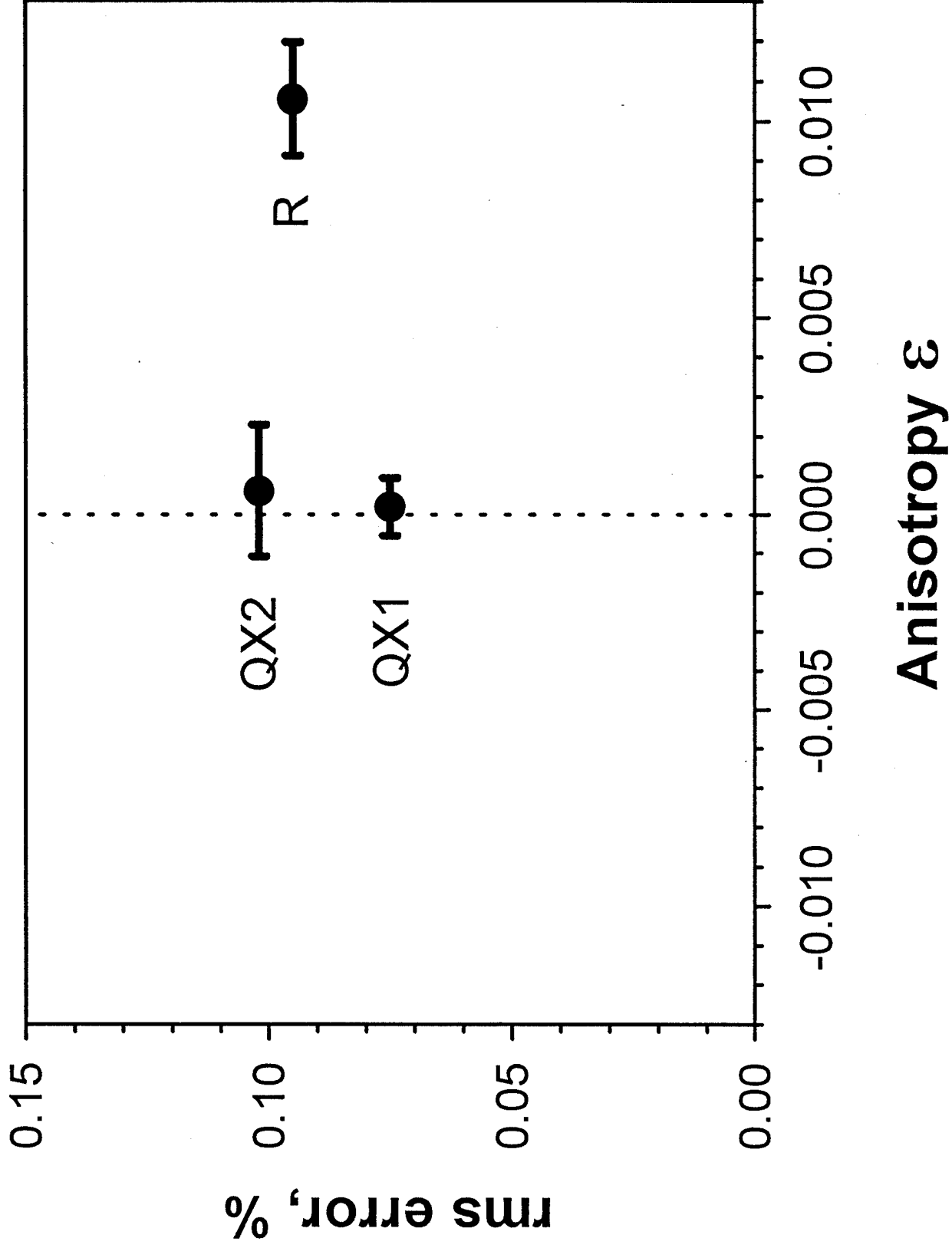
TABLE I. The elastic constants (in Mbar) and anisotropy  $\epsilon$  for R-phase cubic approximant, high-quality quasicrystalline, and lesser quality quasicrystalline AlCuLi. The analysis of normal-mode frequency data for each sample assumes cubic symmetry and three independent elastic constants; a small value for  $\epsilon$  indicates that only two constants are independent. The standard deviations are from Monte Carlo simulations; the absolute accuracy of the elastic constant determination is limited by the errors in dimensions and mass (about 1%).

Sample	$c_{11}$	$c_{12}$	$c_{44}$	$\epsilon^a$	rms error <sup>b</sup> , %
R	1.112	0.311	0.396	$0.0105 \pm 0.0014$	0.09
QX1	1.122	0.304	0.409	$0.0002 \pm 0.0007$	0.07
QX2	1.152	0.314	0.419	$0.0006 \pm 0.0017$	0.10

<sup>a</sup>Anisotropy, from Eq. (1)

<sup>b</sup>See Eq. (2)





## Appendix B.

# Resonant photoacoustic measurements of very low optical absorption in solids

Wei-li Lin, J.D. Maynard

*Department of Physics, Pennsylvania State University University Park, PA 16802*

### Abstract

In this paper, a novel resonant photoacoustic technique is described for measuring very low optical absorption in glass and crystal. A 15-W near infrared Nd:YAG cw laser modulated at the acoustic resonant frequency of the sample generates a resonant acoustic signal amplified by its quality factor. With typical quality factor in the order of  $10^5$ , and by supporting the sample at the corners between two piezoelectric (PVDF) thin film transducers, an optical absorption coefficient on the order of  $10^{-7}\text{cm}^{-1}$  at  $1.06\mu\text{m}$  has been measured with a signal-to-noise ratio of  $\sim 20$ . With a modulated laser of  $\sim 10\text{-W}$ , this technique is capable of measuring optical absorption on the order of  $10^{-9}\text{cm}^{-1}$ .

### 1. INTRODUCTION

Highly transparent materials are the indispensable components in both fundamental research and industry, for example, optical fibers in long distance communication systems. Developments in fabrication have produced new transparent solids with optical absorption coefficient  $\alpha$  on the order of  $10^{-7}\text{cm}^{-1}$  (Ref.1). On the other hand, at long wavelength region, the dominant optical absorption mechanism is rayleigh scattering, which has a scattering cross section inversely proportional to  $\lambda^4$  (Ref.2). As a result, near infrared, glass and crystal absorb light the least, which is why an infrared light is usually employed in an optical

fiber communication system. To detect such a small absorption, faster and more sensitive methods are required.

There are many different techniques in measuring optical absorption, such as transmission<sup>3,4</sup>, and calorimetry<sup>3,5</sup> techniques, and each method has its own limitation and different degree of sensitivity. For a centimeter sized sample, photoacoustic(PA)<sup>3,6-8</sup> technique has been proved to be the most sensitive method in measuring low optical absorption, but its sensitivity is still limited due to the high power laser light scattered onto the attached transducers. Previously, a noncontact resonant PA technique<sup>9</sup> has been reported with remarkably improved sensitivity comparing with conventional PA methods. Instead of a high power pulsed laser( $\sim 10^{-1}$ J) used in the conventional PA technique, a much less power( $\sim 10^{-4}$ J/cycle) cw Argon gas laser at 514.5nm is employed as a light source, and its intensity is modulated at the resonant frequency of a sample. When driven at resonance, the sample itself acts as a natural amplifier. As a result, signal gains a mechanical quality factor  $Q$ , while intrinsic noise of transducers without any gain. For highly transparent and pure samples, such as crystalline quartz,  $Q \simeq 10^4 \sim 10^6$ , which is more than compensates for the lower laser power, and results in  $10 \sim 10^2$  times improved sensitivity.

In previous measurement, the PA signal is detected by an interdigital capacitance transducer without any contact with the sample, which may lead to an optimum  $Q$  value, and a signal-to-noise ratio of 1000 for a quartz sample of  $\alpha \sim 10^{-5} \text{ cm}^{-1}$  at 514.5nm has been achieved. However, this method requires precise positioning of the sample, transducers, and separate sample supports, and it does not work as well near infrared, where  $\alpha$  is near the lowest. Recently, these difficulties have been reduced through the use of  $9\mu\text{m}$  thick PVDF film transducers. By supporting the sample at the corners between two film transducers, the need for separate supports is eliminated, with only a small reduction in the quality factor of the resonance. Instead of an Argon gas laser, a 15-W cw Nd:YAG laser at 1060nm is used to measure possibly the lowest optical absorption of crystalline quartz, which is still used as the testing material due to its high transparency near the infrared, and its very high  $Q$ (as high as  $10^6$ ).

## 2. COMMENTS ON THE RESONANT PHOTOACOUSTIC MECHANISM

**Basic PA mechanism** Photoacoustic phenomenon was first discovered by Bell at the end of last century<sup>10</sup>, and the complete theories of various PA generation mechanism have been formulated since 1960s. For the PA generation in a quartz crystal by a low power laser, the dominant mechanism is thermal expansion effect<sup>11</sup>. When a modulated laser is incident on an optically absorbing material, the temperature and thus the volume of the irradiated area will vary with time due to the energy conversion of absorbed laser power into thermal energy, and due to thermal expansion. The change in the density then causes strain in the local elastic field, generating an acoustic wave in the medium. If the laser is modulated at the resonant frequency of the sample, the sample will be driven to resonance, and the generated acoustic signal will be amplified by Q.

If a modulated laser with power  $W_0$  is aligned passing through the center of a sample, the voltage output of a transducer placed at the corner of the sample is:<sup>9</sup>

$$\Delta V = M\Psi|_{corner} \quad (1)$$

$$= M \left[ \frac{\alpha\beta W_0}{2\pi^{5/2}\rho v C_p} \frac{4aQ}{\pi b} \right] \quad (2)$$

where,  $\Psi$  is the displacement of the sample,  $a$  and  $b$  are the length and height of the sample,  $\rho$  the density,  $\beta$  the thermal expansion coefficient,  $v$  the sound speed in the sample medium,  $C_p$  the heat capacity, and  $M$  the sensitivity of transducers.

Then, optical absorption coefficient can be derived as:

$$\alpha = \frac{\pi^{7/2}}{2} \left[ \frac{\rho v C_p}{\beta W_0} \right] \left[ \frac{b}{aQ} \right] \left[ \frac{\Delta V}{M} \right] \quad (3)$$

From above results, in order to improve the measurement sensitivity, i.e., to measure smaller  $\alpha$  under a fixed noise level corresponding to  $\Delta V$ ,  $Q$  and  $W_0$  should be maximized. Several procedures have been taken to improve  $Q$ , which will be discussed in detail in the next section, while  $W_0$  can be improved by optimizing the laser modulation efficiency, and using multiple beam pass.

**Piezoelectric transduction** Since quartz is a piezoelectric material, when it has a displacement, an electric field along certain orientation will be induced. A piezoelectric transducer, such as a PVDF film, placed at the end of the sample, will not only detect the displacement of the sample itself, it will also pick up this electric field as an antenna. Therefore, the detected PA signal will be greatly enhanced due to the piezoelectric nature of the material.

### 3. APPARATUS

**Setup overview** An illustration of the experiment setup is shown in Fig.1, and Fig.2 shows a sample and its supporting assembly in more details. Two  $9\mu\text{m}$  thick piezoelectric (PVDF) films, typically  $\sim 3.0\text{cm}$  long and  $\sim 0.2\text{cm}$  wide, are used as transducers, and the space between them can be adjusted by motorized positioners. The typical sample is a rectangular parallelepiped, and is supported by the two transducers only at its corners.

A 15-W Nd:YAG cw laser ( $\lambda=1.06\mu\text{m}$ ) is employed as a light source, which is amplitude modulated at the resonant frequency of the sample by an acousto-optic modulator. The modulated laser beam is guided by an optical system so as to pass through the center of the sample. The generated photoacoustic signal is amplified by a preamplifier, and a phase lock-in amplifier is used to reject the noise. The signal is then stored in a computer and plotted on a recorder.

**Improvement on quality factors** The essence of the resonant photoacoustic technique is the multiplication of the received signal by quality factor of a sample. The maximization of quality factor is thus very desirable.

The mechanical quality factor for an oscillating system at resonance can be defined as:

$$Q = 2\pi \frac{E}{\Delta E} \quad (4)$$

where  $E$  is the total energy for the system and  $\Delta E$  is the energy loss per cycle. Internal friction and flaw, surface viscosity, air viscosity, sound radiation, and loss through supports

are the possible causes for the energy losses in the system, which are minimized by several procedures.

Each time before the experiment, the sample is cleaned using pump air and a ultrasonic cleaner. During the alignment, the sample is handled very carefully, with gloves and clean tissues, to avoid any possible damage and dust which may contribute to surface viscosity.

To reduce the energy loss through the supports, the sample is carefully mounted such that only its opposite corners point contact with PVDF transducers. The space between PVDF films and the orientation of the sample will be adjusted by motorized positioners untill the maximum  $Q$  is achieved.

To further minimize the loss due to air viscosity and sound radiation, the sample and its supporting assembly are put inside a vacuum chamber during the experiment. With a mechanical pump, vacuum of  $10^{-3}$  torr can be achieved. Fig.3 shows the improvement on the quality factor for a quartz sample in the vacuum. Typically,  $Q$  on the order of  $10^5$  has been obtained in the vacuum, which is more than four times larger than that in the air.

#### 4. RECIPROCITY CALIBRATION OF THE TRANSDUCERS

Since the sample is supported by two identical PVDF transducers(reversible) at ends, and the laser is acting as a driver, the situation is ideal for a reciprocity calibration to determine the transducer sensitivity  $M^{12}$ . The calibration procedure is as following.

At first, without using the laser, one of the transducers, PVDF1, is used as a source, which will drive the sample into resonance, and the other transducer, PVDF2, is used as a receiver. At resonance, the voltage output of PVDF2,  $V_2'$ , and the current through PVDF1,  $I_1$ , are measured(Fig.4 (a)). Then, the laser is used to generate the resonant acoustic signal in the sample, and both transducers are used as receivers (i.e., PVDF1 is reversed), which give output  $V_1$  and  $V_2$ (Fig.4(b)). The sensitivity can then be calculated as:<sup>12</sup>

$$M = \rho C \omega \left( \frac{V_2' V_2}{Z I_1 V_1} \right)^{1/2} \quad (5)$$

where,  $Z$  is the acoustic transfer impedance, defined as the ratio of the pressure at the

transducer to the volume velocity at the acoustic source, and, for a sample with length  $a$  and height  $b$ , is given as:

$$Z = \frac{\rho C Q}{ab\pi} \quad (6)$$

## 5. ELECTRIC DRIVE MEASUREMENTS

To test the system and to calibrate the transducer, the sample is first driven to resonance by an ac electric signal instead of a modulated laser source. After the sample is in place, one of the PVDF transducers, acting as a source, is connected to a frequency synthesizer. While sweeping the driving frequency, the output from the other PVDF transducer is monitored until resonance occurs. Resonant frequency  $f_0$ , quality factor  $Q$ , and signal amplitude at resonance (referenced as  $V'_2$  in the last section) are then obtained. The quality factor is determined by:

$$Q = \frac{f_0}{(f_2 - f_1)} \quad (7)$$

where,  $f_1$  and  $f_2$  are the frequencies where the transducer signal drops by  $\sqrt{2}$  from its peak value.

To calibrate the transducer using the reciprocity method, the current flowing through the driving transducer (denoted as  $I_1$  in the last section) at resonance is also measured. A capacitance bridge is used to determine the capacitances of the driving PVDF thin film transducer and the cable connecting the transducer to the frequency synthesizer, the capacitance of a PVDF transducer is typically  $\sim 1.5$  pF. By measuring the current entering the cable-PVDF system using an oscilloscope, the current passing through the PVDF transducer can be determined by the current distribution between the transducer and the cable.

The results of quartz resonance by an electric excitation are shown in Table I.

## 6. PHOTOACOUSTIC SIGNAL MEASUREMENTS

After determining  $f_0$  and  $Q$  using electric excitation, a 15-W cw Nd:YAG laser at  $1.06\mu\text{m}$  is used as a driver, and it is first aligned to pass through an acousto-optic modulator with its modulation frequency set by a frequency synthesizer. To achieve a high modulation efficiency, the modulator is mounted on a translation-rotation platform to enable fine adjustment. After proper adjustment, the zeroth-order beam, corresponding to dc component, is blocked, and the modulated first-order beam, typically  $\sim 6\text{watt}$ , is then aligned to pass through the center of the sample by a beam steering system.

By sweeping the modulation frequency over the region containing the resonant frequency of the sample, the resonant photoacoustic signal is excited and may be detected by either PVDF transducer. The maximum values of the PA signal at resonance from both transducers,  $V_1$  and  $V_2$ , are then used to calibrate the transducer and to determine the optical absorption coefficient using equation (3).

After testing the system in the air, the sample and its supporting assembly are then put inside a vacuum chamber. It is found that the PA signal in the vacuum is much larger than that in the air, due to the fact that the quality factor has been much improved in the vacuum. To check the PA mechanism, the PA signal is also measured as a function of the laser power. Measurement results and calculated absorption coefficients will be discussed in detail in the next section.

## 7. RESULTS AND DISCUSSION

It is already known that crystalline quartz with a higher  $Q$  may have a lower optical absorption<sup>13</sup>. Meanwhile, higher  $Q$  also means better PA signal. Thus, quartz crystal with the highest possible  $Q$ , referenced as sample "1" ( $4.0 \times 1.0 \times 1.0\text{cm}$ ), is selected in this project, which may yield possibly the lowest optical absorption  $\alpha$  near infrared. To compare PA results with different samples, another less pure quartz crystal, referenced as sample

"2" (4.5x1.1x1.6cm), is also used.

From previous noncontact PA measurement, sample "1" has a Q of  $8.5 \times 10^5$ , and a  $\alpha$  of  $2.9 \times 10^{-5} \text{cm}^{-1}$  at 514.5nm, while sample "2" has a lower Q,  $6.0 \times 10^5$ , and a higher  $\alpha$ ,  $2.2 \times 10^{-4} \text{cm}^{-1}$ .

In our corner-contact measurement, the noise level is found to be  $\sim 15 \text{nv}$  in the vacuum, while the resonant PA signal is  $\sim 350 \text{nv}$  for sample "1", and  $\sim 12 \mu\text{v}$  for sample "2". Both samples have lower measured Q of  $1.7 \times 10^5$ , which is probably due to the energy loss from the contact support. However, sample "1" has an extremely low measured  $\alpha$  of  $1.8 \times 10^{-7} \text{cm}^{-1}$  using 4.8watt modulated laser at 1060nm, with a signal-to-noise ratio of  $\sim 20$ . The PA signal vs modulated laser frequency for this sample is shown in Fig.5, with resonance occurring at 134383.6Hz. Since the measurement lower limit is proportional to  $\frac{\alpha}{(S/N)/W}$ , with such a signal-to-noise ratio and a modulated laser power of  $\sim 10\text{-W}$ , this method should be able to detect  $\alpha$  as low as  $10^{-9} \text{cm}^{-1}$ , which is a significant improvement over existing techniques on measuring highly transparent crystals.

On the other hand, Fig.6 shows the PA signal vs modulated laser frequency for sample "2", which has a signal-to-noise ratio of  $\sim 800$ . The measured  $\alpha$  is  $1.9 \times 10^{-6} \text{cm}^{-1}$ , i.e., one order of magnitude higher than that of sample "1", which agrees well with the difference in  $\alpha$  for these two samples at visible region(514.5nm). The results of measured  $\alpha$  are summarized in Table II, where, the column labeled W is the modulated laser power in watt, M is the PVDF transducer sensitivity determined by reciprocity calibration in unit of voltage per meter, and  $\frac{\Delta V}{M}$  is the detected displacement at the end of the sample at resonance, in angstroms.

Fig.7 shows the PA signal measured as a function of modulated laser power. It can be seen that the PA signal extrapolates along a straight line, indicating that linear effect is dominant in the conversion of laser power into acoustic energy. However, this straight line does not exactly pass through zero, which implies that there is some electrical pick-up between PVDF films into the PA signal, which maybe eliminated using a metal plate shielding two transducers.

## 8. SUMMARY

A corner contact resonant PA technique have been developed for measuring very small optical absorption. By using several energy loss minimization procedures, especially by supporting the sample between two PVDF transducers at its corners, the quality factor on the order of  $10^5$  has been achieved, which is comparable with that of a noncontact PA technique. Meanwhile, precise positioning and complicated supports, used in noncontact methods, are avoided, and very low  $\alpha$  near infrared can be detected with a good sensitivity. The best signal-to-noise ratio for a quartz sample of  $\alpha \sim 10^{-6}$  is  $\sim 800$ . The lowest  $\alpha$  measured is  $1.8 \times 10^{-7} \text{cm}^{-1}$  at 1060nm with a signal-to-noise ratio of  $\sim 20$ . If a cw laser with a modulated power of  $\sim 10$ -W, this technique is capable of measuring  $\alpha$  on the order of  $10^{-9} \text{cm}^{-1}$  near infrared. These results show that our technique is very promising in measuring extremely low optical absorption in solids.

## ACKNOWLEDGMENTS

This research was sponsored by the NSF Grant No. DMR-9000549 and by the Office of Naval Research.

## REFERENCES

1. M.E. Lines, "The search for very low loss fiber-optic materials," *Science* **226**, 663 (1984).
2. J.J. Sakurai, "Advanced quantum mechanics," Addison-Wesley, 50 (1967).
3. A. Hordvik, "Measurement techniques for small absorption coefficients: recent advances," *Appl. Opt.* **16**, 2827 (1977).
4. K. Jinguji, M. Horiguchi, and T. Manabe, "Spectral loss measurement system for IR optical fibers," *Appl. Opt.* **21**, 571 (1982).
5. R.T. Swimm, Y. Xiao, and M. Bass, "Calorimetric study of optical absorption of Suprasil W-1 fused quartz at visible, near IR and near UV wavelengths," *Appl. Opt.* **24**, 322 (1985).
6. A. Hordvik and H. Schlossberg, "Photoacoustic technique for determining optical absorption coefficients in solids," *Appl. Opt.* **16**, 101 (1977).
7. A. Rosencwaig and T.W. Hindley, "Photoacoustic measurements of low level absorption in solids," *Appl. Opt.* **20**, 606 (1981).
8. Y. Bae, J.J. Song, and Y.B. Kim, "Photoacoustic detection of nanosecond-pulse-induced optical absorption in solids," *Appl. Opt.* **21**, 35 (1982).
9. C. Yu, M.J. McKenna, J.D. Whilt, and J.D. Maynard, "A new resonant photoacoustic technique for measuring very low optical absorption in crystals and glasses," *J. Acoust. Soc. Am.* **91**(2), 868 (1992).
10. A.G. Bell, "On the production and reproduction of sound by light" *Am. J. Sci.* **20**, 305 (1880).
11. V.V. Bottom, "Dielectric constants of quartz," *J. Appl. Phys.* **43**, 1493 (1972).
12. J.D. Maynard and C. Yu, "The use of reciprocity to calibrate resonant photoacoustic measurement," *J. Acoust. Soc. Am. Suppl.* **1 86**, S109 (1989).

13. D.M. Dodd and D.B. Fraser, "The 3000-3900 $\text{cm}^{-1}$  absorption bands and an elasticity in crsyatlline  $\alpha$ -quartz," J. Phys. Chem. Solids **26** 673 (1965).

## FIGURES

Fig. 1. Diagram of the experimental configuration for measuring optical absorption coefficient using the corner-contact resonant photoacoustic technique

Fig. 2. Diagram of the resonant photoacoustic apparatus. The sample is supported by two PVDF film transducers at its corners. The space between transducers and the orientation of the sample can be adjusted by motorized positioners

Fig. 3. Typical resonance curves for a quartz sample using an ac electric excitation, in air and in vacuum. The quality factor is improved by a factor of 4 in vacuum.

Fig. 4. Diagram of the reciprocity calibration of transducers. (a). electric excitation: one transducer, PVDF1, is acting as a driver, and the other one, PVDF2, is used as a receiver. (b). laser excitation: laser is employed as a driver, and both transducers are used as receivers.

Fig. 5. PA resonant curve for quartz sample "1" excited with a modulated laser. The measured optical absorption  $\alpha$  reaches  $1.8 \times 10^{-7} \text{ cm}^{-1}$  at 1060nm.

Fig. 6. PA resonant curve for quartz sample "2" excited with a modulated laser. The signal-to-noise ratio is  $\sim 800$  for a  $\alpha$  of  $1.9 \times 10^{-6} \text{ cm}^{-1}$ .

Fig. 7. PA signal amplitude versus modulated laser power. Extrapolation along a straight line indicates linear effect is dominant in the PA generation.

TABLES

Table 1. Size, resonant frequency  $f_0$ , and quality factor  $Q$  of quartz crystals used in this study. Here,  $a$ ,  $b$ , and  $c$  are the length, height, and thickness of the samples.

<i>Sample</i>	$a$ (cm)	$b$ (cm)	$c$ (cm)	$f_0$ (Hz)	$Q$ ( $\times 10^5$ )
1	4.0	1.0	1.0	134383.60	1.73
2	4.5	1.1	1.6	119793.40	1.74

Table 2. Results of the measurement of optical absorption coefficient of quartz sample using corner-contact resonant photoacoustic technique at 1060nm, where,  $W_0$  is the modulated laser power,  $M$  is the PVDF transducer sensitivity, and  $\Delta V/M$  is the measured sample displacement.

<i>Sample</i>	$W_0$ (W)	$M^a$ ( $\times 10^6 V/m$ )	$\Delta V/M$ (Å)	$\alpha$ ( $\times 10^{-6} cm^{-1}$ )
1	4.8	37.4	0.00009	0.18
2	3.0	81.0	0.00063	1.87

<sup>a</sup>determined by reciprocity calibration

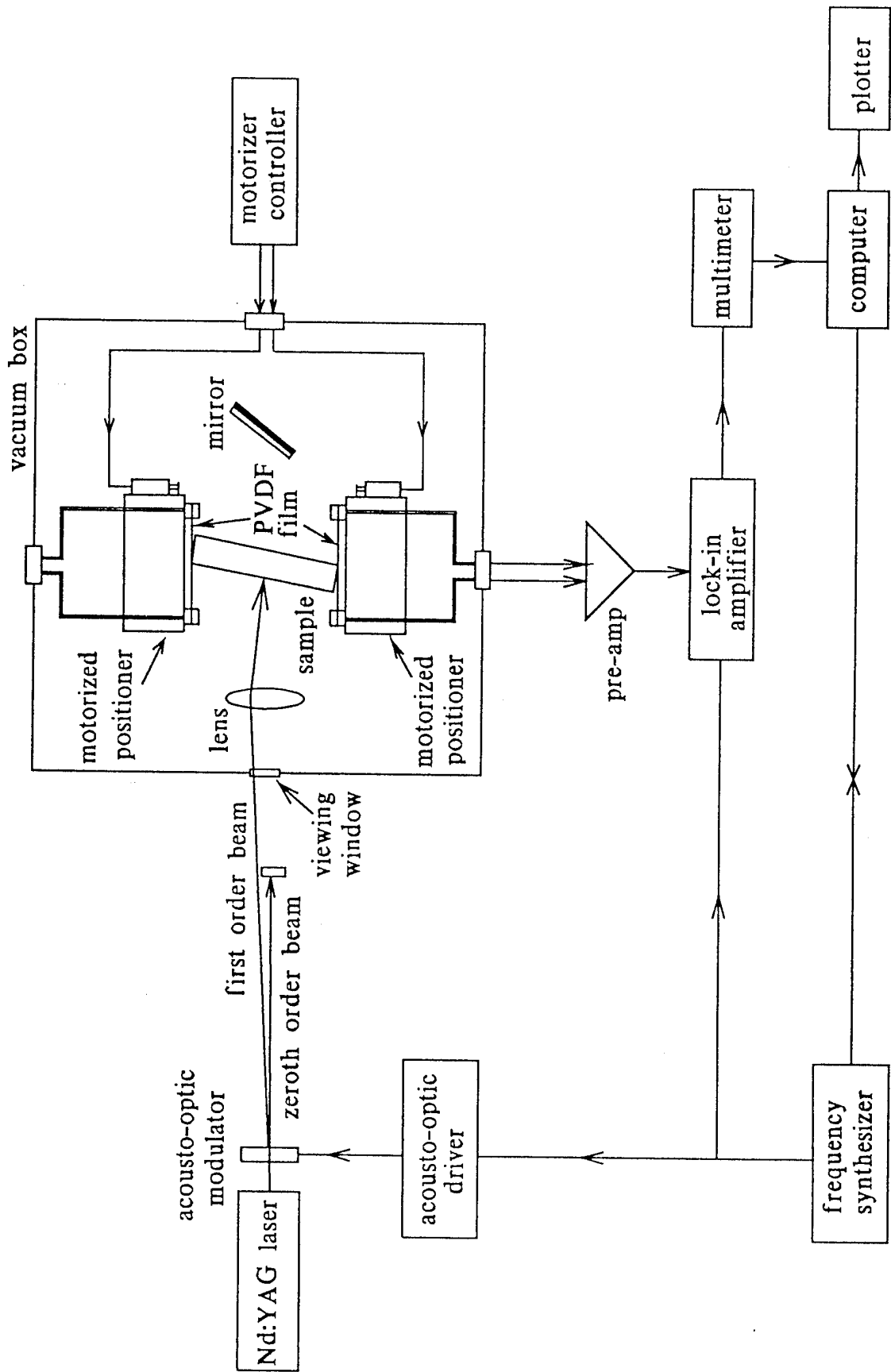


Fig. 1

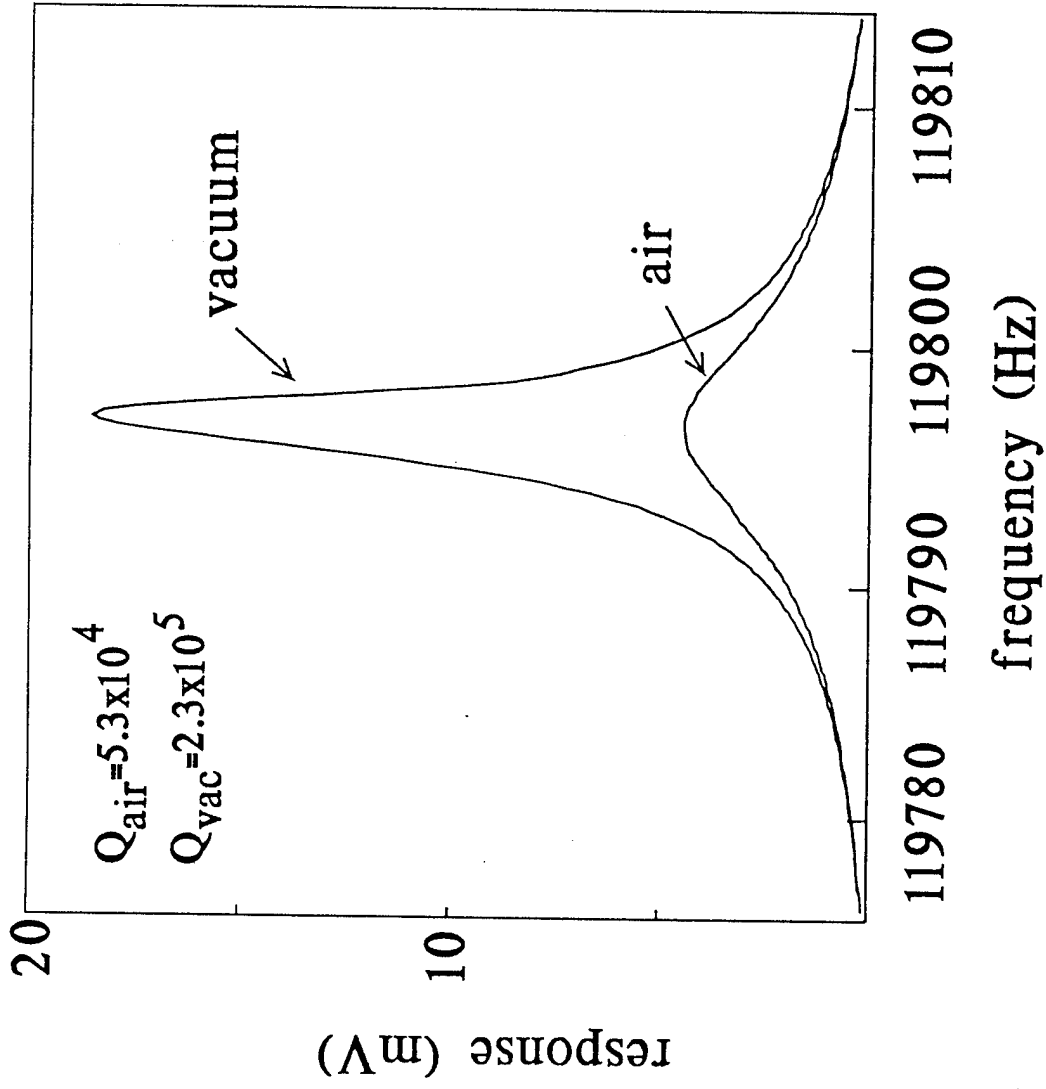
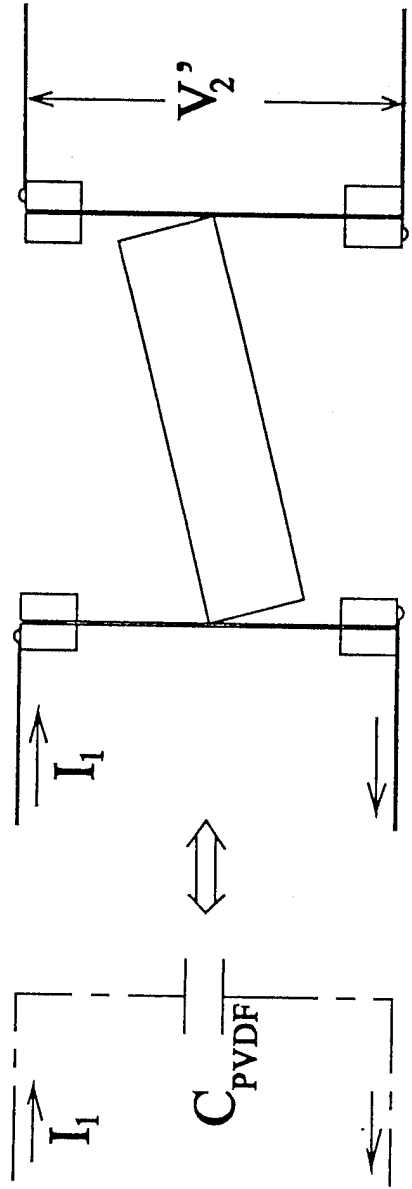
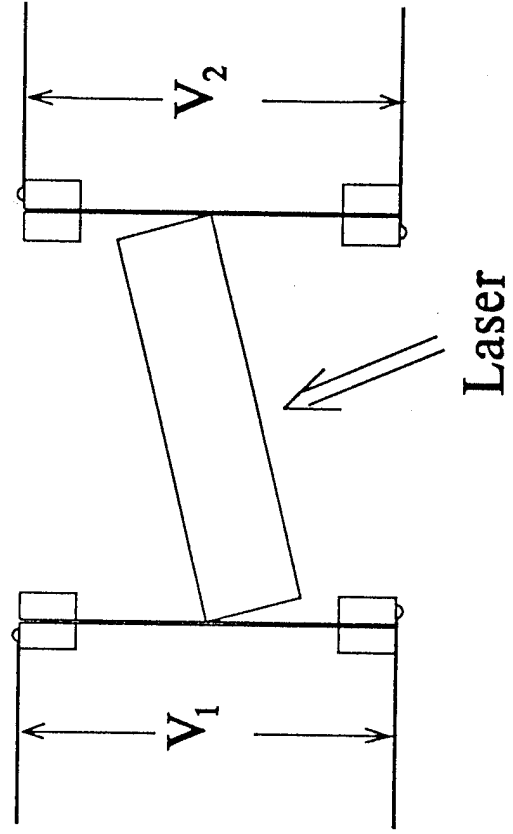


Fig. 3



(a)



(b)

Fig. 4

# Appendix C.

OFFICE OF NAVAL RESEARCH  
PUBLICATIONS / PATENTS / PRESENTATIONS / HONORS REPORT  
for  
01 JUNE 1994 through 31 MAY 1995

R&T Number: 4126941—09  
Contract/Grant Number: N00014-92-J-1186/N00014-93-1-0779/N00014-93-1-1127  
Contract/Grant Title: Innovative Acoustics Techniques for Studying New Materials and new Developments in Solid State Physics, ASSERT, and Anisotropic heat-exchanger/stack configurations for thermoacoustic heat engines  
Principal Investigator: Julian D. Maynard  
Mailing Address: 104 Davey Lab  
University Park, PA 16802  
Phone Number: (814) 865-6353  
E-Mail Address: maynard@phys.psu.edu

- a. Number of Papers Submitted to Refereed Journals: 1
- b. Number of Papers Published in Refereed Journals: 0
- c. Number of Books or Chapters Submitted but not yet Published: 0
- d. Number of Books or Chapters Published: 0
- e. Number of Printed Technical Reports & Non-Refereed Papers: 0
- f. Number of Patents Filed: 1
- g. Number of Patents Granted: 0
- h. Number of Invited Presentations at Workshops or Prof. Society Meetings: 7
- i. Number of Presentations at Workshops or Prof. Society Meetings: 4
- j. Honors/Awards/Prizes for Contract/Grant Employees: 1
- k. Total Number of Graduate Students and Post-Docs Supported at least 25 % this year on this contract/grant:

Grad Students: 4                      and Post-Docs: 1  
Grad Student Female: 0              and Post-Docs Female: 1  
Grad Student Minority: 0            and Post-Docs Minority: 0

## PUBLICATIONS, PRESENTATIONS, ETC.

### PAPERS SUBMITTED TO REFEREED JOURNALS

1. P. S. Spoor, J. D. Maynard, and A. R. Kortan, "Elastic Isotropy and Anisotropy in Quasicrystalline and Cubic AlCuLi", submitted to Phys. Rev. Lett.

### PATENTS/APPLICATIONS

Patent Disclosure, "Stack/Heat-exchanger Unit for Thermacoustic Heat Engines", July 1995

### INVITED PRESENTATIONS AT TOPICAL OR SCIENTIFIC/TECHNICAL SOCIETY CONFERENCES

1. Colloquium, University of Utah, Department of Physics, Salt Lake City, Utah, January 26, 1995, "Tuning-up a Quasicrystal", Orest Symko, host
2. Seminar, Department of Physics, Ohio State University, Columbus, OH, March 1, 1995, "Tuning-up a Quasicrystal", Will Saam, host
3. Seminar, Acoustics Program, Penn State University, University Park, PA February 7, 1995, "Tuning-up a Quasicrystal", Ken Gilbert, host
4. Invited lecture series, Physical Acoustics Summer School, Pacific Grove, CA, June 1994, "Periodic, random, and quasiperiodic media"
5. P. S. Spoor and J. D. Maynard, Workshop on Resonant Ultrasound Spectroscopy, University of Wisconsin, MI, August 1994, "Use of Piezoelectric films and RUS on small samples of novel materials"
6. Society of Physics Students, Zone 3 Meeting, Penn State University, April 8, 1995, "Tuning-up a quasicrystal", Bruce Wyatt, host
7. Wei-li Lin, "Resonant photoacoustic measurement of optical absorption in solids", J. Acoust. Soc. Am. **97**, 3408 (1995)

### CONTRIBUTED PRESENTATIONS AT TOPICAL OR SCIENTIFIC/TECHNICAL SOCIETY CONFERENCES

1. P. S. Spoor and J. D. Maynard, "Elastic-constant determination of small, near-isotropic crystals using resonant ultrasound spectroscopy: New quasicrystal results", J. Acoust. Soc. Amer. **96**, 3226 (1994)
2. T. Zhang, S. R. Savitski, and J. D. Maynard, "Observation of individual bond breaking events in the onset and propagation of fracture", J. Acoust. Soc. Amer. **96**, 3227 (1994)

3. L. C. Krysac, T. Zhang, and J. D. Maynard, "The fracture of brittle carbonaceous form as a candidate for a physical realization of the random fuse model for material breakdown", Bull. Am. Phys. Soc. **40**, 478 (1995)
4. P. S. Spoor and J. D. Maynard, "Numerical anomalies in the Rayleigh-Ritz method for calculating the normal mode vibrations of arbitrarily shaped elastic solids", J. Acoust. Soc. Am. **97**, 3326 (1995)

### **HONORS/AWARDS/PRIZES**

J. D. Maynard was awarded the Silver Medal in Physical Acoustics by the Acoustical Society of America, November, 1994

### **GRADUATE STUDENTS SUPPORTED UNDER CONTRACT FOR YEAR ENDING 31 OCTOBER 1995**

1. Philip Spoor (Ph.D. candidate, acoustics) began Fall 1989, Elastic Constant Measurements for Quasicrystals
2. Wei-Li Lin (Ph.D. candidate, physics) began summer 1991, Infrared resonant photoacoustics
3. David Chao Zhang (Ph.D. candidate, physics) began summer 1994, Thermoacoustic heat engines
4. Brian Bennett (Ph.D. Candidate, Acoustics Program) began summer 1994, Superfluid hydrodynamics in a capillary array

### **POSTDOCTORALS SUPPORTED UNDER CONTRACT FOR YEAR ENDING 31 OCTOBER 1994**

1. Tian-ming Zhang, Postdoctoral Scholar, began June, 1994
2. Cindy Krysac, Postdoctoral scholar, began July, 1994

### **MISCELLANEOUS**

Undergraduates Involved in Research:

1. Joseph Buck, Junior, 1994-95
2. John Lelii, NSF Research Experience for Undergrad. student 1995
3. Kirk Fisher, Junior, 1994-95
4. Patrick Johnston, 1994-95
5. Mike Marotta, NSF Research Experience for Undergrad. student 1995